Shockless Acceleration of Thin Plates Modeled by a Tracked Random Choice Method

Bradley J. Plohr*
Los Alamos National Laboratory, Los Alamos, New Mexico

A method for accelerating thin metallic plates to hypervelocities has been proposed by G. McCall. In this method, a shock in a propellant generates a strong expansion wave that smoothly accelerates the plate. We have studied the hydrodynamics of this process in one dimension, both analytically and computationally. The metal was modeled as a stiffened gas, and the corresponding Riemann problem was solved. The asymptotic behavior of the solution was determined analytically. The one-dimensional random choice method, modified so that material boundaries are tracked and the spatial mesh is refined locally, was used to compute the flow; comparison with the asymptotic solution demonstrated its accuracy. With this method, shocks that form within the accelerating plate were accurately resolved, so that possible structural damage to the plate could be evaluated.

Introduction

A METHOD for accelerating a thin metal plate to exceedingly high velocities within a short distance has been proposed by McCall.[1] These hypervelocities, on the order of 1 cm/μs, are difficult to achieve without destroying the plate since the kinetic energy of the plate exceeds its vaporization energy. The acceleration must be rapid enough to attain high velocities within a short distance, on the order of 10 cm, but it must be sufficiently smooth that strong shock waves do not form inside the metal. Furthermore, the compression of the plate resulting from the acceleration must be relieved gradually so that the plate does not spall.

A schematic diagram of the experimental configuration proposed by McCall is shown in Fig. 1. A tube containing a tungsten plate is partially filled with a plastic foam (CH) that serves as a propellant; a low-pressure cavity separates the foam from the plate. The energy needed to accelerate the plate is supplied by a planar shock passing through the foam and compressing it. When the shock reaches the end of the foam, the foam expands isentropically into the cavity. At the leading edge of this rarefaction wave is a low-density, high-velocity material, which is followed by material with gradually increasing density and decreasing velocity. As succeedingly denser portions of the foam reach the plate, the pressure behind the plate rises, thereby gradually accelerating the plate. Thus, the low-pressure cavity intervening between the foam driver and the plate converts the shock wave in the foam into a strong rarefaction wave that smooths the acceleration. Of course, the rising pressure behind the plate produces compression waves in the plate that, in general, steepen into shock waves. McCall has estimated the formation time for such shock waves and has concluded that shockless acceleration of sufficiently thin plates can be achieved using his method.

A more complete modeling of this hydrodynamic process entails computer simulation. Numerical methods for solving the Euler equations encounter three major difficulties in modeling this flow. First, the mass density varies over a vast range, from the high density in the tungsten plate and the compressed foam to the near-vacuum conditions inside the cavity. Therefore, Lagrangian coordinates, which place few mesh blocks in regions of low density, are inappropriate for the leading edge of the rarefaction wave. On the other hand, the material boundary between the metal and the fluid accelerating it is the focus of interest. Whereas the position of this boundary is naturally tracked in Lagrangian coordinates, it is uncertain to within a mesh length on an Eulerian grid; furthermore, most Eulerian methods exhibit substantial numerical diffusion that spreads the interface over many mesh lengths. Finally, the formation of shock waves within the plate must be detected accurately, even though the metal plate is very thin, spanning only a few computational mesh zones.

In this paper, we have modeled the hydrodynamics of McCall's problem using a combination of methods that address these difficulties. The computation is performed in Eulerian coordinates to allow for arbitrarily low densities in the cavity. To model the material interfaces correctly, their positions are tracked across the Eulerian grid. Also, the computational mesh is refined in the vicinity of the plate to better resolve the flow in this region. Finally, the underlying numerical scheme for solving the flow equations, the random choice method, models shock waves as sharp discontinuities resolved within a mesh block, so that shock formation can be detected within the thin plate. This numerical approach gives solutions of a much higher quality than were previously available.

The plan of the paper is as follows. In the next section, the thermodynamic model used for the tungsten plate is described. Then the solution of the Riemann problem, which is the key input into the random choice method, is described for this thermodynamic model. Next, the random choice method, as extended by front tracking and mesh refinement, is explained. In the subsequent section, analytical results on the short-time behavior of flows in which rarefaction waves impinge on a plate are compared to a numerical solution. Lastly, the results of numerical experiments for McCall's problem are presented.

Thermodynamics

The shockless acceleration of metal plates will be modeled as a hydrodynamic process. This requires the specification of a suitable equation of state for each component substance. Since use of the random choice method requires that Riemann problems be solved, it is advantageous to use an equation of state that is amenable to analytic solution. The propellant may be modeled as a polytropic gas, for which the solution of the Riemann problem is simple, but the metal plate cannot be adequately modeled as such. In lieu of designing a Riemann solver for a general equation of state, such as one based on the SESAME tables,[2] we have modeled the metal plate as a "stiffened gas." This equation of state gives the correct semiquantitative behavior of the plate. In conjunction with a

Received May 12, 1987; revision received Sept. 11, 1987.

*Collaborator, Theoretical Division; currently, Assistant Professor, Computer Sciences Department and Center for the Mathematical Sciences, University of Wisconsin, Madison, WI.

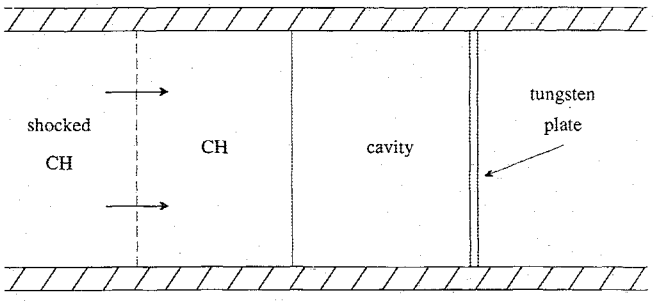

Fig. 1 Schematic diagram of the shockless acceleration of a tungsten plate using a plastic foam (CH) propellant.

spall model to give yield strains and an estimate of melting and boiling points, it can be used to assess the feasibility of shockless acceleration.

The equation of state for a stiffened gas[3] is given by the relation

$$E = [1/(\gamma - 1)]\ [(p + \gamma p_\infty)/\rho]$$

between the specific (internal) energy E, the pressure p, and the mass density ρ. Here γ and p_∞ are prescribed constants that characterize the gas, γ being dimensionless and p_∞ being a pressure.

The isentropes for a stiffened gas may be determined by noting that

$$T\mathrm{d}S = \mathrm{d}E + p\mathrm{d}\left(\frac{1}{\rho}\right) = \frac{p + p_\infty}{\rho}\,\frac{1}{\gamma - 1}\,\mathrm{d}\,\log\left(\frac{p + p_\infty}{\rho^\gamma}\right) \tag{1}$$

so that $(p + p_\infty)/\rho^\gamma = \text{const}$ along an isentrope. The speed of sound c, defined by

$$c^2 = \left(\frac{\partial p}{\partial \rho}\right)_S = \left(\frac{\partial p}{\partial \rho}\right)_E + \frac{p}{\rho^2}\left(\frac{\partial p}{\partial E}\right)_\rho$$

may be calculated to be

$$c = \left(\gamma\,\frac{p + p_\infty}{\rho}\right)^{1/2} \tag{2}$$

Right- and left-facing rarefaction waves, which correspond to the characteristic speeds $v \pm c$, satisfy the equations $\mathrm{d}v \mp \mathrm{d}p/\rho c = 0$ and $\mathrm{d}S = 0$. By Eqs. (1) and (2), we determine that

$$v \mp [2/(\gamma - 1)]\,c = \text{const} \tag{3}$$

and

$$(p + p_\infty)/\rho^\gamma = \text{const} \tag{4}$$

across rarefactions corresponding to the characteristic speeds

$$v \pm c \tag{5}$$

The Hugoniot locus is given by solving the equation

$$E - E_0 + \frac{1}{2}\,(p + p_0)\left(\frac{1}{\rho} - \frac{1}{\rho_0}\right) = 0$$

for ρ in terms of ρ_0, p_0, and p. Simple algebra yields the result

$$\frac{\rho}{\rho_0} = \frac{(\gamma + 1)(p + p_\infty) + (\gamma - 1)(p_0 + p_\infty)}{(\gamma + 1)(p_0 + p_\infty) + (\gamma - 1)(p + p_\infty)} \tag{6}$$

As for any equation of state, the speed σ of the corresponding right- and left-facing shocks may be determined from the relations

$$\rho(v - \sigma) = \mp m = \rho_0(v_0 - \sigma) \tag{7}$$

where

$$m = \left(-\frac{p - p_0}{1/\rho - 1/\rho_0}\right)^{1/2} \tag{8}$$

is the mass flux across the wave.

To demonstrate the adequacy of using a stiffened gas equation of state to model a metal plate made from tungsten, we compare to experimental data.[4] These data show that a plot of shock speed $U_s = |\sigma - v_0|$ vs particle speed $U_p = |v - v_0|$ along the principal Hugoniot of tungsten is well approximated by a straight line

$$U_s \approx c_0 + \alpha U_p \tag{9}$$

for pressures up to 3 Mbar. Here $c_0 = 0.404$ cm/μs is (approximately) the sound speed in tungsten at standard conditions and $\alpha = 1.23$ is an empirical dimensionless constant. For a general equation of state, one finds from Eqs. (7) and (8) that $U_p/U_s = (\rho - \rho_0)/\rho$ and $U_sU_p = (p - p_0)/\rho_0$. Using the Hugoniot relation (6) for a stiffened gas, one can eliminate p and ρ to find that

$$U_s = \left[c_0^2 + \left(\frac{\gamma + 1}{4}\,U_p\right)^2\right]^{1/2} + \frac{\gamma + 1}{4}\,U_p \tag{10}$$

For our calculations modeling tungsten, we have used $\gamma = 3.14$ and $p_\infty = 1.0$ Mbar. A plot comparing the empirical linear fit to the stiffened gas relation (10) for pressures up to 3 Mbar is shown in Fig. 2. The stiffened gas relation coincides with the linear fit to within 3%.

Riemann Problems

A Riemann problem for a system of conservation laws in one space dimension is an initial-value problem with scale invariant initial data, i.e., data at $t = t_0$ that is constant to either side of a jump discontinuity at $x = x_0$. We use the subscript l to label the initial state on the left of x_0, and r for the initial state on the right of x_0. The solution of a Riemann problem is constant along each ray $\xi = (x - x_0)/(t - t_0) = \text{const}$ through (x_0, t_0); thus, we may specify the solution as a function of the speed ξ.

The solution of a Riemann problem for a stiffened gas requires only a simple modification of the well-known solution for a polytropic gas. It consists of a left-facing (i.e., $v - c$)

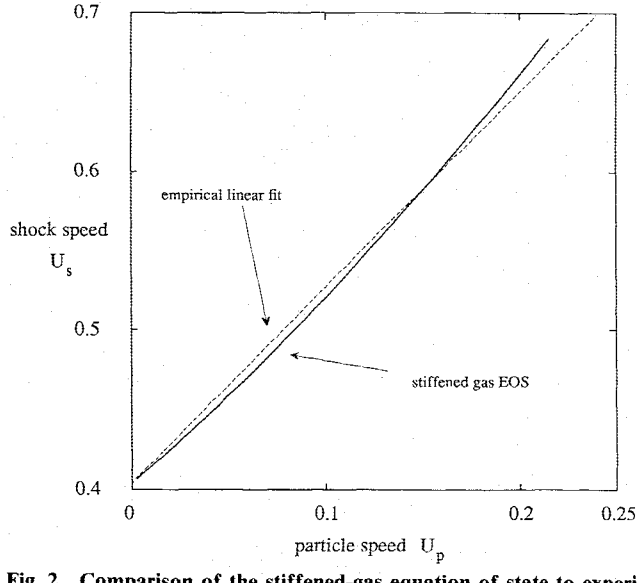

Fig. 2 Comparison of the stiffened-gas equation of state to experimental data for the tungsten.

rarefaction or shock wave on the left, a right-facing (i.e., $v + c$) rarefaction or shock wave on the right, and a contact discontinuity (moving with velocity v) in between, as indicated schematically in Fig. 3. It is convenient to speak of the left side of a left-facing wave and the right side of a right-facing wave as being "ahead" of the wave, the opposite sides being "behind" the wave; the corresponding states are labeled by the subscripts a and b. A left- or right-facing wave is determined by the state ahead of it together with one other parameter, such as the pressure behind it. For the left (respectively, right) wave in the solution of a Riemann problem, the state ahead of the wave is the left (respectively, right) initial state. Since the particle velocity and the pressure are continuous across a contact discontinuity, the velocities and pressures behind the left and right waves must coincide. Thus, solving a Riemann problem amounts to finding the pressure in the middle between the left and right waves such that the particle velocities behind the waves are equal.

For a shock wave, conservation of momentum may be written as

$$\mp m(v_a - v_b) + p_a - p_b = 0 \tag{11}$$

Here m is defined as a function of the pressure p_b behind the shock and the state ahead of the shock through Eqs. (6) and (8), as long as $p_b \geq p_a$. For a rarefaction wave, we may define m through the equation

$$-m\frac{2}{\gamma - 1}(c_a - c_b) + p_a - p_b = 0$$

so that by Eq. (3) we find that Eq. (11) again holds. With this definition and Eqs. (2) and (4), m may be expressed as a function of p_b and the state ahead of the wave, as long as $p_b < p_a$. More explicitly, we have

$$m = [\gamma_a \rho_a (p_a + p_{\infty,a})]^{1/2} \cdot \varphi\left(\frac{p_b + p_{\infty,b}}{p_a + p_{\infty,a}}, \gamma_a\right) \tag{12}$$

where

$$\varphi(r,\gamma) = \frac{\gamma - 1}{2\gamma}\frac{1 - r}{1 - r^{(\gamma-1)/2\gamma}}, \quad \text{if } r < 1$$

$$= \left(\frac{\gamma + 1}{2\gamma} r + \frac{\gamma - 1}{2\gamma}\right)^{1/2}, \quad \text{if } r \geq 1$$

Let v_* and p_* denote the common values of the particle velocity and pressure on the two sides of the contact discontinuity. Then, by Eq. (11), we have

$$-m_r(v_r - v_*) + p_r - p_* = 0$$

and

$$+m_l(v_l - v_*) + p_l - p_* = 0$$

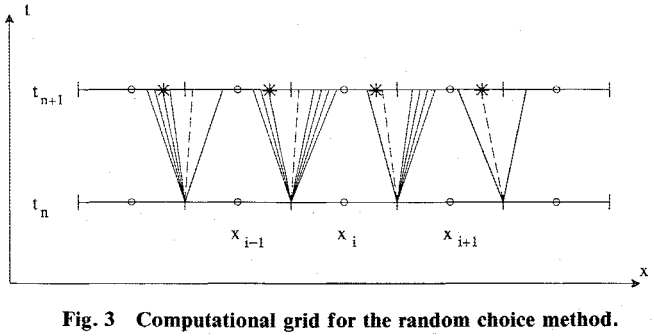

Fig. 3 Computational grid for the random choice method.

for the right and left waves, where m_r is expressed by Eq. (12) in terms of $p_b = p_*$ and the density and pressure ρ_r and p_r ahead of the wave, and similarly for m_l. These equations may be written as

$$p_* = \frac{v_l - v_r}{1/m_l + 1/m_r} + \frac{m_l p_r + m_r p_l}{m_l + m_r} \tag{13}$$

and

$$v_* = \frac{p_l - p_r + m_l v_l + m_r v_r}{m_l + m_r} \tag{14}$$

Therefore, to solve a Riemann problem, we first use the Godunov-Chorin[5,6] fixed-point iteration to solve Eq. (13) for the pressure p_* between the left and right waves. Then, Eq. (14) gives the velocity v_* in the middle, and for both the right- and left-facing waves, the state along a ray moving at a specified speed ξ may be determined using either Eqs. (2–5) or (6) and (7) accordingly as the wave is a rarefaction or a shock. Except for the modifications to the formulas (2), (4), (6), and (12), the construction of the solution of the Riemann problem is identical to that for a polytropic gas (for which $p_\infty = 0$).

Tracked Random Choice Method

The random choice method is a numerical method for solving the general initial-value problem for a system of conservation laws. It is based on the constructive existence proof for solutions of conservation laws of Glimm[7] and was adapted for numerical computation by Chorin.[6] For a recent review of work on the random choice method, see Ref. 8.

In the random choice method for the hyperbolic system of conservation laws

$$u_t + f(u)_x = 0 \tag{15}$$

the solution is determined at the lattice of space-time points (x_j, t_n); here,

$$x_j = (1/2)(x_{j-1/2} + x_{j+1/2})$$

is the center of the mesh cell from $x_{j-1/2}$ to $x_{j+1/2}$. Given the solution values $u_j^n = u(x_j, t_n)$ at time level n, the solution values u_j^{n+1} at level $n + 1$ are determined in three stages.

First, an approximation $u^n(x)$ for the solution at time t_n and an arbitrary position x is reconstructed by defining u^n to be piecewise constant on mesh cells:

$$u^n(x) = u_j^n, \quad \text{if} \quad x_{j-1/2} \leq x < x_{j+1/2} \tag{16}$$

Next, consider solving the initial-value problem for Eq. (15) with initial data [Eq. (16)] at time t_n. For $t - t_n$ sufficiently small, the solution is given in terms of the solutions of a sequence of Riemann problems between the states u_j^n and u_{j+1}^n and centered at the points $(x_{j+1/2}, t_n)$. The situation is depicted in Fig. 3. In fact, the waves in the solutions of the Riemann problems centered at neighboring points $(x_{j-1/2}, t_n)$ and $(x_{j+1/2}, t_n)$ will not interact as long as the Courant-Friedrichs-Levy condition

$$t - t_n < t_{\text{CFL}} = (1/2) \min_j (x_{j+1/2} - x_{j-1/2})/\lambda_j \tag{17}$$

holds, where λ_j is the maximum wave speed, in absolute value, in the solution of the Riemann problem centered at $(x_{j+1/2}, t_n)$. We have taken $t_{n+1} - t_n = C \cdot t_{\text{CFL}}$ with the Courant number C kept between 0.7 and 0.9.

Finally, an equidistributed random number η_{n+1} is chosen from the interval

$$-(1/2) \le \eta_{n+1} < (1/2)$$

and the solution value u_j^{n+1} is taken to be the value $u*$ of the solution of the preceding initial-value problem sampled at the position

$$x* = x_j + \eta_{n+1} \cdot (x_{j+1/2} - x_{j-1/2})$$

at time t_n. In our computations, we have used the Van der Corput sequence[9] to obtain η.

The solution given by the random choice method has the advantage, when compared to standard finite-difference methods, of preserving the structure of discontinuous waves in the solution: shock waves and contact discontinuities remain perfectly sharp. Therefore, the method is able to detect formation of shock waves within regions extending only a few mesh cells. This property is crucial for our application to shockless acceleration of thin plates.

The price paid for perfect resolution of discontinuous waves is that their positions are not exactly correct. On the average, the position of a discontinuous wave in the numerical solution is correct, but the wave performs a random walk about this correct position. To remedy this in situations where maintaining the position of certain prominent waves is critical, Glimm et al.[10] introduced the tracked random choice method.

In a front tracking method, certain waves in the flow, typically strong discontinuous waves, are resolved on a subgrid level. With each tracked front is associated a position and a wave type. The wave type determines how the tracked front moves and interacts with the fluid. For example, in gasdynamics the possible wave types include left- and right-facing pressure waves and contact discontinuities.

Let x_f^n denote the position of a particular tracked front at time t_n. If the tracked front lies in the jth mesh cell at time t_n, i.e., $x_{j-1/2} \le x_f^n < x_{j+1/2}$, then the solution values u_{j-1}^{n+1}, u_j^{n+1}, and u_{j+1}^{n+1} are obtained in a fashion different from that just described. The piecewise constant data u^n is defined by

$$\begin{aligned} u^n(x) &= u_{j-1}^n, \quad \text{if} \quad x_{j-3/2} \le x < x_f^n \\ &= u_{j+1}^n, \quad \text{if} \quad x_f^n \le x < x_{j+3/2} \end{aligned}$$

for x in the interval $x_{j-3/2} \le x < x_{j+3/2}$, and by Eq. (16) for x outside this interval. As before, the initial-value problem with initial data u^n at time t_n is solved up to time t_{n+1}. The position of the tracked front at time t_{n+1} is

$$x_f^{n+1} = x_f^n + s \cdot (t_{n+1} - t_n)$$

where the velocity s is determined according to its wave type. Finally, the solution value u_{j+1}^{n+1} is taken to be the value $u*$ of the solution of this initial-value problem at time t_{n+1} sampled at the position

$$x* = x_{j-3/2} + (\eta_{n+1} + 1/2)\,(x_f^{n+1} - x_{j-3/2})$$

Similarly u_{j+1}^{n+1} is obtained by sampling at

$$x* = x_f^{n+1} + (\eta_{n+1} + 1/2)\,(x_{j+3/2} - x_f^{n+1})$$

The choice for the value of u_j^{n+1} seems somewhat arbitrary. For instance, one could take u_j^{n+1} to be u_{j-1}^{n+1} or u_{j+1}^{n+1} according as $x_j \le x_f^{n+1}$ or $x_f^{n+1} < x_j$. We have found that, with this choice, however, a strong wave crossing the tracked wave does not separate correctly from the tracked wave after the interaction. This effect is rather dramatic in calculations where a tracked shock wave is followed closely by a strong rarefaction wave. To remedy this, we instead define u_j^{n+1} to be u_{f-}^{n+1} or u_{f+}^{n+1} according as $x_j \le x_f^{n+1}$ or $x_f^{n+1} < x_j$, where u_{f-}^{n+1} and u_{f+}^{n+1} are the states on either side of the tracked front.

In gasdynamics, the possible wave types are: contact discontinuities, moving with the particle velocity v; left- and right-facing pressure waves, which either follow sound waves moving with velocity $v \pm c$ in case the solution is continuous across the wave (the rarefaction case), or move with the shock velocity σ if the wave is discontinuous (the shock case); Neumann and Dirichlet boundaries, which supply boundary conditions; and movable walls, which are ascribed a mass density and move according to Newton's law. The velocity of a left- or right-facing pressure wave or contact discontinuity is calculated by solving the Riemann problem between u_{j-1}^n and u_{j+1}^n, centered at (x_f^n, t_n), and determining the velocity of the corresponding wave in this solution. (We track the leading edge of a rarefaction wave.) Neumann and Dirichlet boundaries are stationary, and their interaction with the flow is determined by solving a Riemann problem between the fluid state neighboring the boundary and, respectively, the same state with a reflected velocity or the imposed boundary state. The evolution of a movable wall is determined as follows.

Let the wall have mass per unit area M and velocity v_{wall}^n at time t_n. Suppose, for concreteness, that the fluid lies on the right side of the wall, so that the solution value inside the fluid is $u_r = u_{j+1}^n$. Define the virtual state u_l to have the same pressure and density as u_r and to have the velocity

$$v_l = 2v_{\text{wall}}^n - v_r$$

obtained by reflection through the moving wall. Then solve the Riemann problem between u_l and u_r centered at (x_f^n, t_n) and sample it at the position

$$x* = x_f^n + v_{\text{wall}}^n \cdot (t_{n+1} - t_n)$$

to obtain the state $u*$ on the fluid side of the wall at time t_{n+1}. Because v_l is obtained by reflection, the velocity, $v*$ of the fluid at the wall coincides with v_{wall}^n, so that the correct boundary conditions have been maintained. The pressure in the fluid accelerates the movable wall according to Newton's law. If $\Delta t = t_{n+1} - t_n$ is small enough (more precisely, as may be deduced from the analytic solution,[11] if $p*\Delta t/Mc*$ is small), we may approximate this acceleration by

$$v_{\text{wall}}^{n+1} = v_{\text{wall}}^n + \frac{p_r + p*}{2} \cdot \frac{\Delta t}{M}$$

The speed s of the moving wall during this time interval is then taken to be

$$s = \frac{1}{2}(v_{\text{wall}}^{n+1} + v_{\text{wall}}^n)$$

To obtain acceptable resolution of the waves in the thin plate, the computational grid must be refined in the vicinity of the plate. The positions of the edges of the mesh cells $x_{j+1/2}$, $j = 0,\ldots,N$ are defined as follows. The grid spans the interval $[x_{\min}, x_{\max}]$ and has a subinterval $[a,b]$ over which the mesh is refined by the refinement ratio R. To smooth the transition between the coarse and fine meshes, a mollification parameter ϵ is also specified, with $\epsilon = 0$ corresponding to a sharp transition. We define

$$\begin{aligned} \rho_0(\xi) &= 1/R, \quad \text{if } 0 < \xi < 1 \\ &= 1, \qquad \text{otherwise} \end{aligned} \tag{18}$$

and let ρ_ϵ be the convolution $\rho_\epsilon = \delta_\epsilon * \rho_0$ of ρ_0 with an approximate δ function. We have used

$$\delta_\epsilon(\xi) = \frac{1}{\epsilon}\,\delta_1\left(\frac{\xi}{\epsilon}\right)$$

where

$$\delta_1(\xi) = \frac{1}{\pi(1+\xi^2)}$$

With these definitions, the zone edges are given by

$$x_{j+1/2} = x_{\min} + (x_{\max} - x_{\min}) \cdot \int_{\xi_0}^{\xi_j} d\xi\ \rho_\epsilon(\xi) \Big/ \int_{\xi_0}^{\xi_N} d\xi\ \rho_\epsilon(\xi) \quad (19)$$

where

$$\xi_j = \xi_0 + \frac{j}{N} \cdot (\xi_N - \xi_0)$$

It remains to define ξ_0 and ξ_N. The transitions occurring betwen the coarse and fine meshes at $\xi = 0$ and $\xi = 1$ in Eq. (18) are to correspond to $x = a$ and $x = b$ through Eq. (19). For $\epsilon \neq 0$, this gives a pair of nonlinear equations to be solved for ξ_0 and ξ_N in terms of a and b. When $\epsilon = 0$, however, these equations reduce to linear equations, with the solution

$$\xi_0 = -(1/R)\,[(a - x_{\min})/(b - a)]$$

and

$$\xi_N = 1 + (1/R)\,[(x_{\max} - b)/(b - a)]$$

for simplicity, we use these equations to define ξ_0 and ξ_N.

Analytical Results

As a preliminary to solving the shockless acceleration problem, we study a similar problem for which analytical information is available. This is the problem of the reflection from a rigid wall of a rarefaction wave expanding into a vacuum. The short-time asymptotic solution of this problem has been described by Greenspan and Butler;[12] they reduce the problem to the solution of a boundary-value problem for a system of ordinary differential equations, which they solve numerically. These equations may, in fact, be integrated analytically in terms of incomplete beta functions. This solution is described in another paper.[13]

A flow pattern is shown in Fig. 4. A rarefaction wave in a polytropic gas with adiabatic exponent γ connects the state $\rho = \rho_0$, $p = p_0$, $v = v_0$ to the vacuum $\rho = 0$, $p = 0$; it originates at $x = 0$ at time $t = 0$. The rarefaction wave corresponds to the left-facing (i.e., $v - c$) family of characteristics. The rarefaction arrives at the wall located at $x = x_0$ at time

$$t_0 = x_0\{v_0 + [2/(\gamma - 1)]c_0\}^{-1}$$

whereupon a reflected shock wave forms to decelerate the expanding fluid.

Figure 5 shows a comparison of the analytical results with the results of solving the partial differential equations governing the rarefaction reflection flow. In this problem, $\gamma = 1.4$, $\rho_0 = 1$, $p_0 = 1$, and $x_0 = 1$; the time coordinate is taken to be $\tau = t - t_0$, so the rarefaction strikes the rigid wall when $\tau = 0$. Two calculations were performed, one a free expansion for which $v_0 = 0$, and one in which the expanding material has been shocked to $v_0 = \sqrt{2/\gamma(\gamma - 1)}c_0$, which corresponds to an infinite-strength shock. The short-time asymptotic solution predicts that the pressure at the wall should rise as $(\tau/t_0)^{2/(\gamma-1)}$ and that the speed of the reflected shock should tend to $U_s = 0.036494\ [v_0 + 2c_0/(\gamma - 1)]$. In this computation, the flow in the region $0.9 \le x \le 1$ and $0 \le \tau \le 0.3$ was simulated using 100 mesh cells. Figure 5 shows the agreement with the asymptotic pressure rise, and a contour plot of pressure in the space-time plane shows that the reflected shock speed agrees as well. One may ascertain that the short-time asymptotic solution is valid for $\tau/t_0 < 0.1$, roughly speaking.

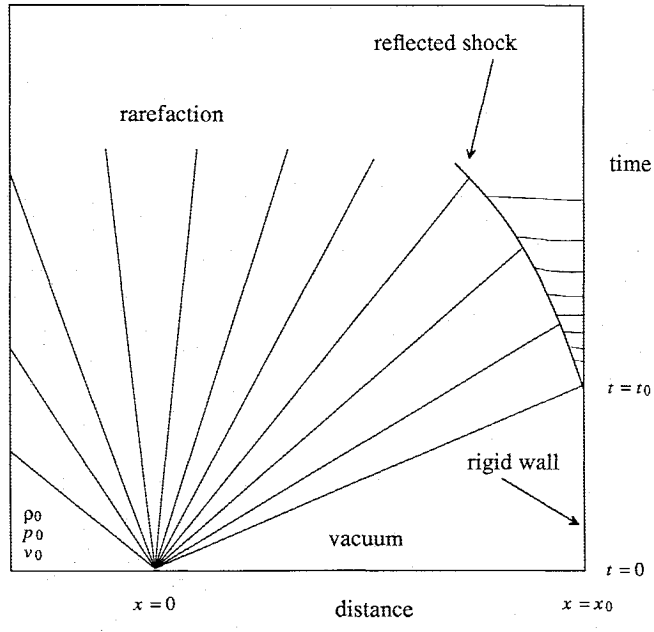

Fig. 4 Reflection of a rarefaction from a rigid wall.

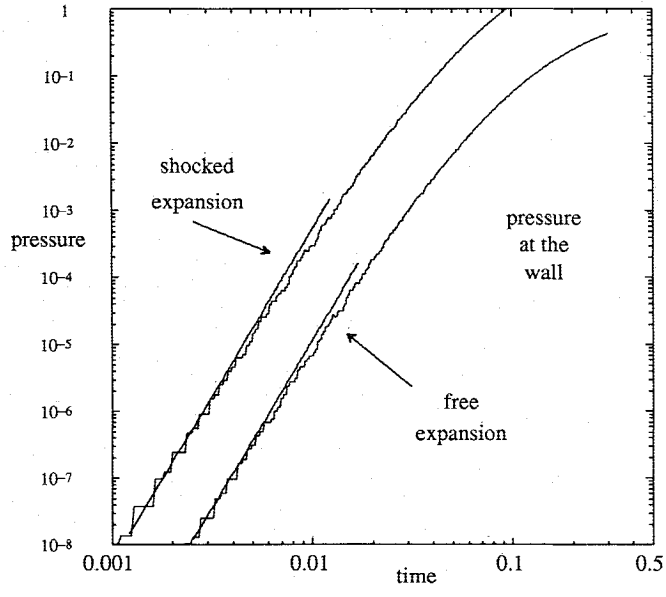

Fig. 5 Pressure at the wall for the reflection of rarefaction wave expanding into a vacuum.

We point out that the random choice solution is accurate over more than 8 decades in pressure; this contrasts with serious discrepancies, over only 3 decades in pressure, among several numerical methods applied to this problem, as reported by McCall.[1]

Suppose now that the wall is replaced with a thin metallic plate that is allowed to accelerate. The behavior of the pressure at the plate is the same as for a rigid wall until the plate has accelerated significantly. The rising pressure generates a compressive wave inside the plate, and we wish to determine whether this wave collapses into a shock wave within the plate.

Simple geometry shows that the sound characteristics inside the plate will cross within the plate if

$$\delta x = c^2 \Big/ \frac{dc}{dt}$$

is less than the thickness of the plate. If the plate is modeled as a stiffened gas with adiabatic exponent γ_0, then

$$\delta x = \frac{2\gamma_0}{\gamma_0 - 1} c \cdot \left(p + p_\infty\right) \Big/ \frac{\mathrm{d}p}{\mathrm{d}t} \tag{20}$$

because the flow is isentropic. For the self-similar solution to this problem,

$$p = (\tau/t_0)^{2/(\gamma-1)}\, \hat{p}[(x - x_0)/\tau]$$

with $\hat{p}$ given by inverting incomplete beta functions, so in the limit $p \ll p_\infty$,

$$\delta x = \frac{2\gamma_0}{\gamma_0 - 1} c_\infty \left(\frac{p + p_\infty}{p_\infty}\right)^{(\gamma_0 - 1)/2\gamma_0} \cdot \frac{\gamma - 1}{2} \frac{p + p_\infty}{p} \tau$$

$$\approx c_\infty t_0 \cdot \gamma_0 \frac{\gamma - 1}{\gamma_0 - 1} \frac{p_\infty}{\hat{p}(0)} \left(\frac{\tau}{t_0}\right)^{-(3-\gamma)/(\gamma-1)}$$

where c_∞ denotes the sound speed in the plate at zero pressure.

When $\gamma = 5/3$ and the propellant material has been shocked with an infinite-strength shock, $\hat{p}(0)$ may be calculated to be $\hat{p}(0) = 51.678 p_0$. Therefore, if we consider tungsten ($c_\infty = 0.404$ cm/μs, $\gamma_0 = 3.14$, $p_\infty = 1$ Mbar) accelerated by plastic foam that has been shocked to $p_0 = 0.24$ Mbar and $\rho_0 = 0.12$ g/cm^3 and that is separated from the plate by a 5-cm gap, one calculates that $\delta x > 0.5$ cm during the initial stages of the acceleration, $\tau < 0.1 t_0 \approx 0.06$ μs. This agrees with the estimate given by McCall.[1]

Computational Results

Figures 6–8 present the results of a shockless acceleration experiment in which the cavity has been evacuated to 10^{-4} bar (the remaining fluid being a gas, with $\gamma = 5/3$). The foam, which is modeled as a polytropic gas with $\gamma = 5/3$, is initially at atmospheric pressure and density 0.03 g/cm^3. The foam is then shocked to 0.24 Mbar and 0.12 g/cm^3; the particle velocity in the shocked foam is 2.45 cm/μs.

In this computation, the tungsten plate is tracked, with the plate modeled as a movable wall with an areal mass density of 0.5 g/cm^2, corresponding to a thickness of 0.025 cm. A 3:1 mesh refinement is used for $4 < x < 6$ cm, with a total of 300 mesh cells: the mesh spacing near $x = 5$ cm is $\Delta x \approx 0.013$ cm, while near $x = 10$ cm it is $\Delta x \approx 0.035$ cm.

Figure 6 shows the space-time development of the flow in terms of the contours of pressure. At time $t = 0$, the shock reaches the end of the foam at $x = 0$, whereupon the foam expands into the cavity. A very weak shock, which is not visible in these plots, is transmitted into the gas in the cavity and leads the expanding foam; its arrival at the tungsten plate is indicated in the figure. The foam decelerates when it strikes the plate, so a reflected shock forms and strengthens. The increasing pressure in the foam that builds up behind the plate serves to accelerate the plate.

The pressure behind the tungsten plate is plotted as a function of time in Fig. 7. Because the cavity has been evacuated, the pressure rise is much smoother than if no cavity had been there. The velocity of the tungsten plate is plotted as a function of time in Fig. 8. The velocity of the plate at $t = 3.85$ μs is 2.69 cm/μs.

Figure 7 may be used to obtain another estimate for the crossing distance for characteristics in the plate. The rate-of-

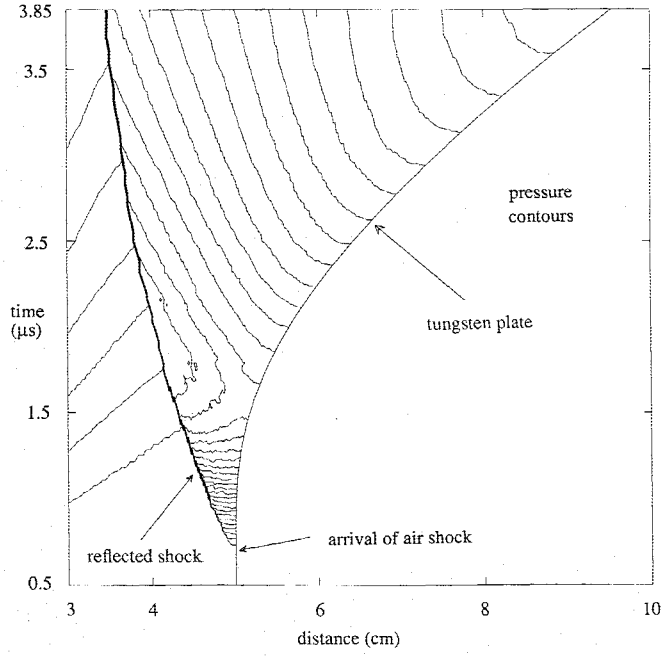

Fig. 6 Pressure contours for shockless acceleration using an evacuated cavity.

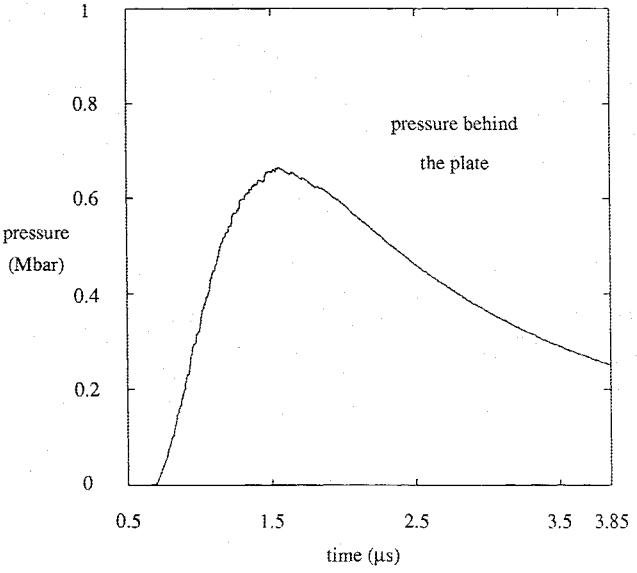

Fig. 7 Pressure behind the plate.

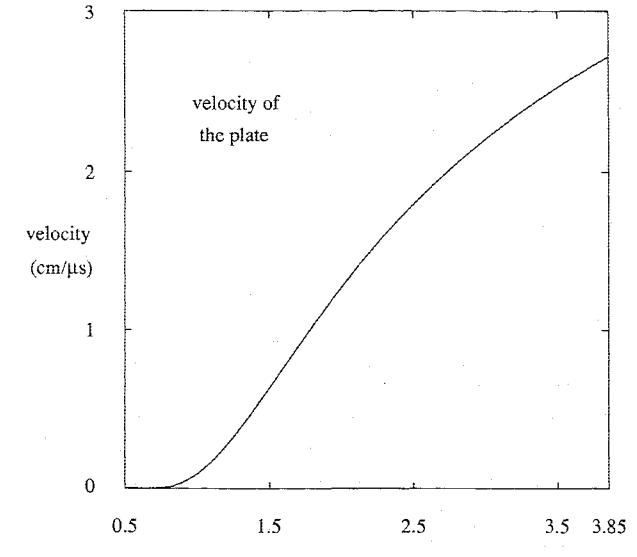

Fig. 8 Velocity of the plate.

pressure rise is estimated from the graph to be $dp/dt \approx 1.1$ Mbar/μs, so Eq. (20) gives

$$\delta x > \frac{2\gamma_0}{\gamma_0 - 1} c_\infty \cdot \frac{p_\infty}{dp/dt} \approx 1 \text{ cm}$$

which is 40 times the thickness of the plate.

Figures 9–11 present the results of a shockless acceleration experiment in which the cavity is filled with air (with $\gamma = 5/3$) at standard conditions. The foam is shocked as in the previous computation. In this computation, both the foam-air contact and the tungsten plate are tracked. The tungsten plate is modeled as a movable wall with an area mass density of 0.5 g/cm^2. A 3:1 mesh refinement is used for $4 < x < 6$ cm, as before.

Figure 9 shows the space-time contours of pressure. Because the cavity is not evacuated, the weak shock that is transmitted to the air has more noticeable effects; its arrival at the plate is marked by a shock reflected from the plate. The contact discontinuity between the foam and the air interacts with waves reflected from the plate, which strengthen into a reflected shock that overtakes the expansion wave in the foam. A layer of compressed air moving with the plate separates the foam from the plate.

There is much more structure in the flow near the plate in this computation as compared to the previous one. The succession of shock waves reflecting between the foam–air contact discontinuity and the tungsten plate can be seen clearly in Fig. 9. Some waves are not visible in this figure, but are evident in a contour plot of the density; the principal feature is a secondary contact discontinuity in the foam that parallels the foam–air interface.

The pressure behind the tungsten plate is plotted as a function of time in Fig. 10. The smooth rise in pressure seen in Fig. 7 has now become jagged during the early stages of the flow development, and the peak pressure is higher. The pressure jump at $t = 0.87$ is caused by the air shock hitting the plate, and the jumps that follow correspond to the succession of shock waves that reflect from the plate, as seen in Fig. 9. The hump at $t \approx 1.7$ corresponds to the arrival at the plate of signals from the right edge of the expansion wave in the foam; this is also seen in Fig. 9. Figure 11 shows the velocity of the tungsten plate plotted as a function of time. The kinks in this plot correspond to the discontinuities in Fig. 10. The velocity of the plate at $t = 3.85$ μs is again 2.69 cm/μs.

Although the short-time development of the flow changes markedly when the cavity pressure is raised to a pressure as small as 10^{-6} Mbar, the long-time behavior of the flow and the accelerating plate are little affected. This is evident in the contour plots and the plots of the velocity of and pressure behind the plate. In fact, at late times, the velocity and pressure for the air-filled cavity agree quantitatively with these quantities when the cavity is evacuated.

The reverberating shock waves that are present in the flow when the cavity has not been evacuated may cause damage to the accelerating plate, for instance, through shock heating. To ascertain the effect that these air shocks have on the plate, the experiment with the air-filled cavity was simulated, during the early stages of the interaction, with the tungsten plate modeled as a thin (0.025 cm) layer of fluid. In this computation, the equation of state of the tungsten is a stiffened gas, with $\gamma = 3.14$ and $p_\infty = 1.0$ Mbar. The two sides of the plate are tracked, as is the foam-air contact discontinuity. A 10:1 mesh

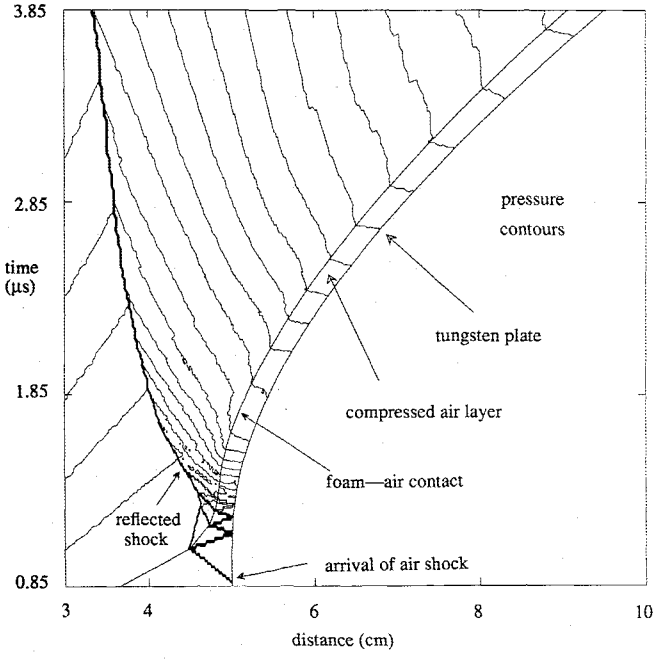

Fig. 9 Pressure contours for shockless acceleration using an air-filled cavity.

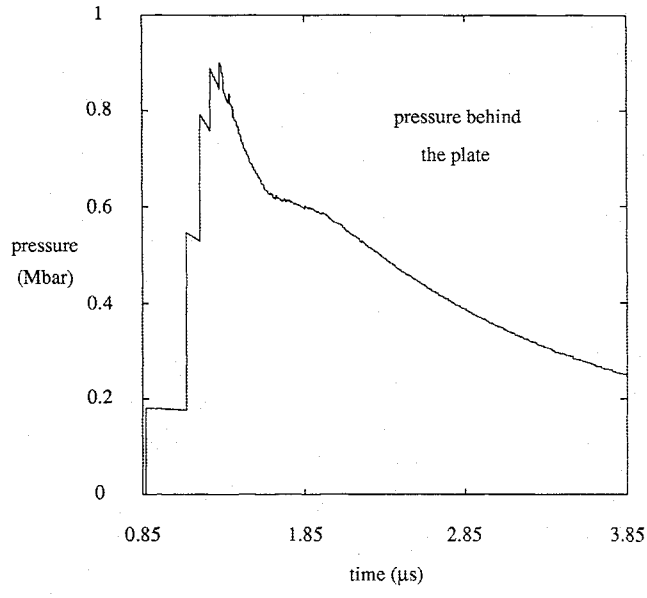

Fig. 10 Pressure behind the plate.

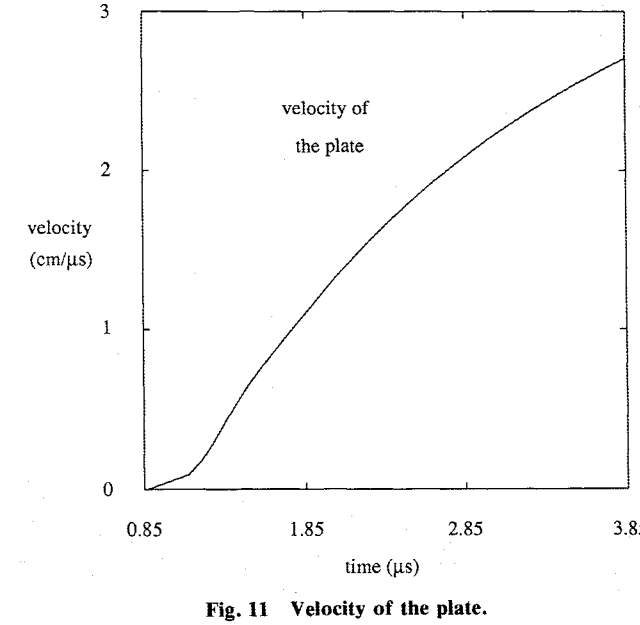

Fig. 11 Velocity of the plate.

refinement is used for $4.95 < x < 5.25$ cm, with a total of 300 mesh cells. With this mesh refinement, there are approximately 10 mesh cells inside of the plate.

The results are shown in Figs. 12–16. Figure 12 shows the space-time contours of pressure, in which the shocks that form inside the plate are evident. An expanded view of the pressure contours in the vicinity of the accelerating plate is shown in Fig. 13. The detailed internal structure of the flow inside the plate is evident in this plot. The corresponding plot of the pressure behind the plate, plotted as a function of time, is shown in Fig. 14. The pressure jump at $t = 0.87$ is caused by the air shock hitting the plate, and the jumps that follow correspond to the succession of shock waves that reflect from the plate, as seen in Figs. 15 and 16.

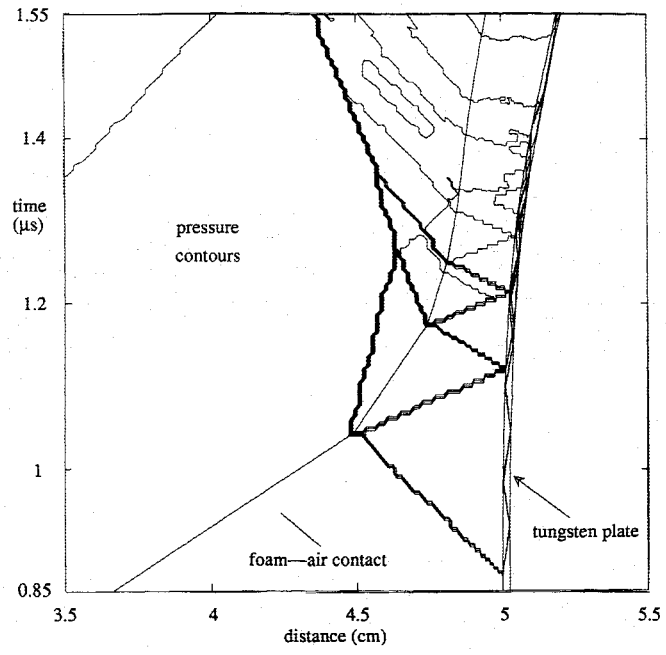

Fig. 12 Pressure contours for shockless acceleration using an air-filled cavity.

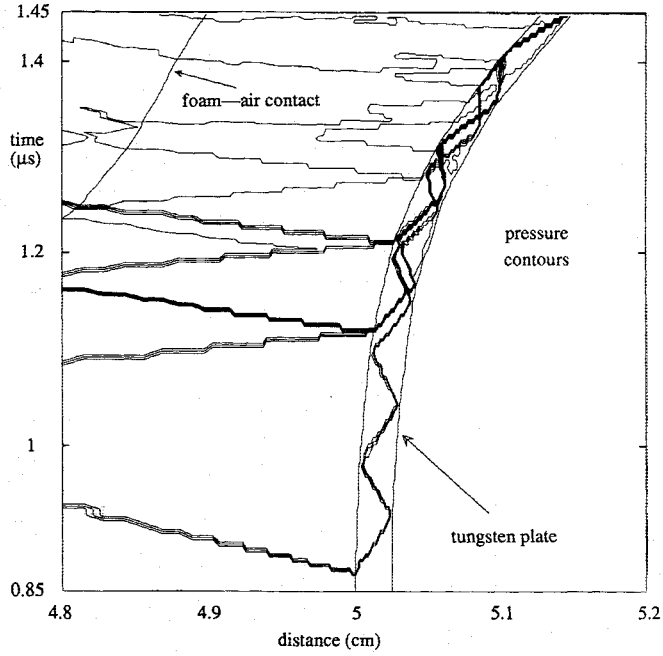

Fig. 13 Expanded view of the plate.

The relative velocity of the two sides of the plate is plotted as a function of time in Fig. 15. A positive relative velocity indicates expansion of the plate. The jumps in the expansion velocity correspond to waves in the air arriving at the plate and to waves in the plate reflecting from the ends of the plate, as seen in Fig. 13. Shock waves in the air that strike the back end of the plate transmit a shock wave into the plate and cause the relative velocity to drop. The transmitted shock reflects from the front end of the plate as a rarefaction wave and causes the relative velocity to rise. This simple ringing of the plate continues until interactions between waves create broad rarefaction waves that complicate the flow.

Although the ringing of the plate is rather violent, the rarefaction waves never continue to put the material in tension, as they do in a spall experiment. (This is confirmed by plotting the minimum pressure in the plate as a function of time.) Within the confines of this simplistic model for the equation of state, therefore, it is expected that the plate will not spall when it is accelerated in the manner being investigated.

As another diagnostic measure for possible structural damage to the plate, the heat deposition in the plate due to

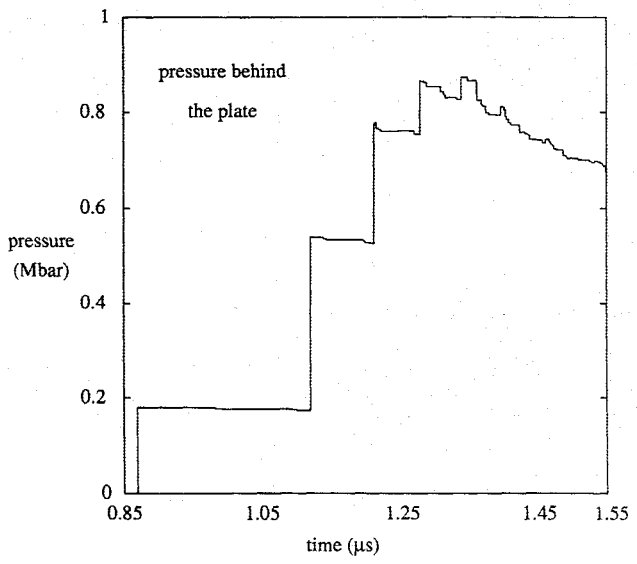

Fig. 14 Pressure behind the plate.

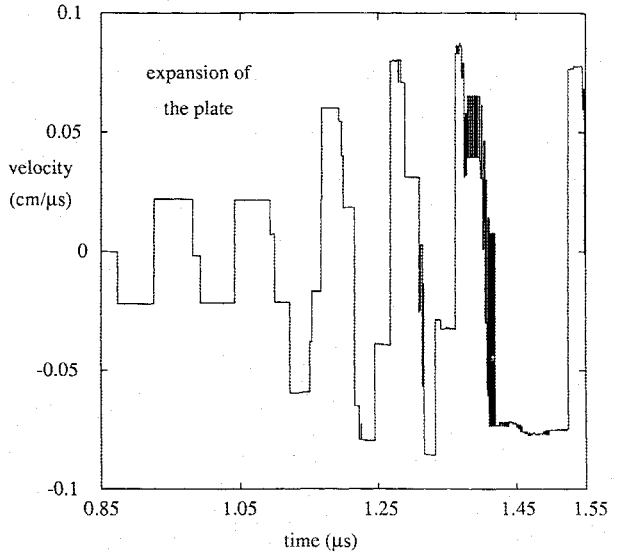

Fig. 15 Expansion of the plate.

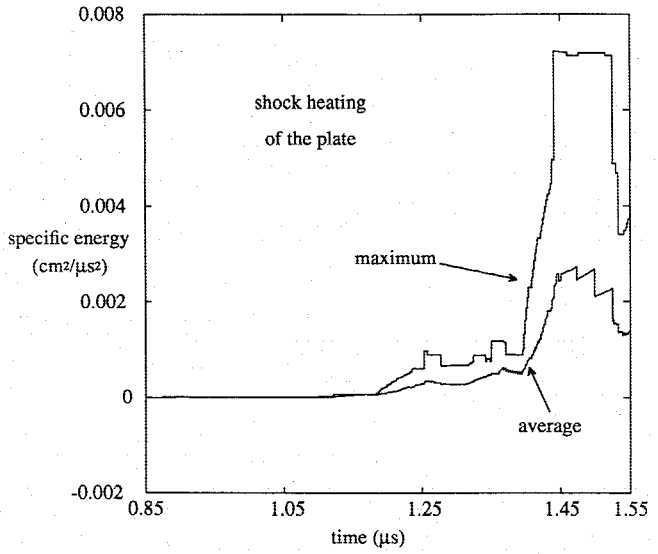

Fig. 16 Shock heating inside the plate.

shock waves should be determined. This heat deposition is to be compared to the heat of melting of tungsten to determine whether the plate melts. Since the plate is being accelerated by a light fluid, it is subject to Rayleigh-Taylor instability. Were the plate to melt, its material strength might not sufficiently dampen the growth of these instabilities, and it could be destroyed.

The stiffened-gas equation of state is not complete, in that the temperature and entropy is not determined. In place of using a complete equation of state, an approximation to the heat deposition in the plate is determined by comparing the computed specific energy in the plate with the specific energy that would be in the plate if the plate had been isentropically compressed. Let

$$E = [1/(\gamma - 1)][p + p_\infty + (\gamma - 1)p_\infty/p]$$

be the specific energy in a given computational mesh cell inside the plate, and let

$$E_{S_0} = [1/(\gamma - 1)][(\rho/\rho_0)^\gamma(p_0 + p_\infty) + (\gamma - 1)p_\infty/\rho]$$

be the corresponding specific energy of the cell were it to have been compressed isentropically from its initial state with density ρ_0. [See Eq. (1).] We then define

$$\Delta Q = E - E_{S_0} \approx T\Delta S$$

to be an effective heat deposition in the cell. The maximum of this quantity over the plate and its spatial average is plotted as functions of time in Fig. 16. Since the latent heat of fusion of tungsten at standard conditions is 0.0019 $cm^2/\mu s^2$, which is of the same order of magnitude as ΔQ, no definitive conclusion can be drawn from the calculation, although it suggests that the plate might melt.

Conclusions

These computations demonstrate the ability of our numerical method to resolve the highly complicated flows that arise in McCall's method for accelerating thin plates. The combination of mesh refinement, front tracking, and the random choice method is crucial to resolving shock waves propagating inside the plate.

The short-time asymptotic solution and the computational results confirm that shock waves do not form inside a sufficiently thin plate, provided that the cavity between the propellant foam and the plate has been evacuated. The computations do show, however, that it is critical to have a good vacuum in the cavity: pressures of only 10^{-6} on the scale of pressures being considered give rise to significant shock waves in the plate. These shock waves cause violent ringing of the plate but they never put the plate into tension; thus, according to the model used, the plate does not spall. The shock waves also heat the plate, and a simple estimate of this effect indicates that the plate might melt. This melting would make the plate more susceptible to Rayleigh-Taylor instability.

In combination with a better model of the structural properties of the tungsten plate, the results of these hydrodynamic calculations can be used to more conclusively determine the feasibility of McCall's method for shockless acceleration of thin plates.

Acknowledgments

This work was sponsored by the U.S. Department of Energy, the U.S. Army under Contract DAAG29-80-C-0041, and the National Science Foundation under Grant DMS-8601766. The author is grateful to R. Menikoff for contributing many ideas in the physical interpretation of the numerical results. He also thanks J. Glimm and D. Sharp for their support and encouragement.

References

[1]McCall, G., "A Method for Producing Shockless Acceleration of Masses to Hypervelocities Using High Explosives," Rept. LJI-TM-84-106, La Jolla Inst., La Jolla, CA, May 1984.

[2]*T-4 Handbook of Material Properties Data Bases, Vol. 1c: Equations of State,* edited by K. Holian, Los Alamos National Lab., Los Alamos, NM, 1984.

[3]Harlow, F. and Amsden, A., "Fluid Dynamics," LANL Monograph LA-4700, 1971.

[4]*LASL Shock Hugoniot Data,* edited by S. Marsh, Univ. of California Press, Berkeley, CA, 1980.

[5]Godunov, S., "A Difference Method for Numerical Calculation of Discontinuous Solutions of the Equations of Hydrodynamics," *Matematicheskii Sbornik,* Vol. 47, 1959, pp. 271–306.

[6]Chorin, A., "Random Choice Solutions of Hyperbolic Systems," *Journal of Computational Physics,* Vol. 22, 1976, pp. 517–533.

[7]Glimm, J., "Solutions in the Large for Nonlinear Hyberbolic Systems of Equations," *Communications on Pure and Applied Mathematics,* Vol. XVIII, 1965, pp. 697–715.

[8]Saito, T. and Glass, I., "Application of Random-Choice Method to Problems in Gasdynamics," *Progress in Aerospace Science,* Vol. 21, 1984, pp. 201–247.

[9]Colella, P., "Glimm's Method for Gas Dynamics," *SIAM Journal on Scientific and Statistical Computing,* Vol. 3, 1982, pp. 76–110.

[10]Glimm, J., Marchesin, D., and McBryan, O., "Subgrid Resolution of Fluid Discontinuities II," *Journal of Computational Physics,* Vol. 37, 1980, pp. 336–354.

[11]Love, A. and Pidduck, F., "Lagrange's Ballistic Problem," *Transactions of the Royal Society of London,* Vol. 222, 1922, pp. 167–226.

[12]Greenspan, H. and Butler, D., "On the Expansion of a Gas into a Vacuum," *Journal of Fluid Mechanics,* Vol. 13, 1962, pp. 101–119.

[13]Plohr, B., "Modeling of Shockless Acceleration of Thin Plates Using a Tracked Random Choice Method," MRC Tech. Summary Rept. 2968, 1987.